Monthly Notices of the ROYAL ASTRONOMICAL SOCIETY

Mon. Not. R. Astron. Soc. **423,** 478–485 (2012) doi:10.1111/j.1365-2966.2012.20891.x

A photometric and spectroscopic study of NSVS 14256825: the second sdOB+dM eclipsing binary★

L. A. Almeida,† F. Jablonski, J. Tello and C. V. Rodrigues

Instituto Nacional de Pesquisas Espaciais/MCTI, Av. dos Astronautas 1758, São José dos Campos, SP 12227-010, Brazil

Accepted 2012 March 8. Received 2012 March 8; in original form 2012 January 13

ABSTRACT

We present an analysis of $UBVR_CI_CJH$ photometry and phase-resolved optical spectroscopy of NSVS 14256825, an HW Vir type binary. The members of this class consist of a hot subdwarf and a main-sequence low-mass star in a close orbit ($P_{\rm orb} \sim 0.1$ d). Using the primary-eclipse timings, we refine the ephemeris for the system, which has an orbital period of 0.110 37 d. From the spectroscopic data analysis, we derive the effective temperature, $T_1 = 40\,000 \pm 500$ K, the surface gravity, $\log g_1 = 5.50 \pm 0.05$, and the helium abundance, $n(\rm He)/n(\rm H) = 0.003 \pm 0.001$, for the hot component. Simultaneously modelling the photometric and spectroscopic data using the Wilson–Devinney code, we obtain the geometrical and physical parameters of NSVS 14256825. Using the fitted orbital inclination and mass ratio ($i = 82\overset{\circ}{.}5 \pm 0\overset{\circ}{.}3$ and $q = M_2/M_1 = 0.260 \pm 0.012$, respectively), the components of the system have $M_1 = 0.419 \pm 0.070\,{\rm M}_\odot$, $R_1 = 0.188 \pm 0.010\,{\rm R}_\odot$, $M_2 = 0.109 \pm 0.023\,{\rm M}_\odot$ and $R_2 = 0.162 \pm 0.008\,{\rm R}_\odot$. From its spectral characteristics, the hot star is classified as a subdwarf OB (sdOB) star.

Key words: binaries: eclipsing – stars: fundamental parameters – stars: individual: NSVS 14256825 – stars: low-mass – subdwarfs.

1 INTRODUCTION

HW Virginis (HW Vir) systems consist of a subdwarf B or OB (sdB or sdOB; hereafter referred to as sdB) plus a main-sequence star, which form an eclipsing pair in a compact orbit, $P_{\rm orb} \sim 0.1$ d (Heber 2009). These systems are believed to evolve through a common-envelope (CE) phase when the primary (sdB) is a red giant. During this stage, the secondary star (dM) spirals in towards the primary one and the potential gravitational energy released is absorbed by the envelope, which is subsequently ejected (Taam & Ricker 2010). The final separation between the dM and the sdB stars depends on the initial mass ratio of the binary and the initial separation.

sdB stars consist of a helium-burning core covered by a thin hydrogen-dominated envelope. The atmosphere abundance is normally $n(\rm He)/n(\rm H) \sim 0.01$, the effective temperatures are in the range of 22 000–37 000 K, and the logarithmic surface gravities are normally between 5.2 and 5.7. They populate a narrow strip on the extreme horizontal branch (EHB) in the Hertzsprung–Russell diagram. The single-star stellar evolution predicts a narrow mass range: $0.46 - 0.50\,{\rm M}_\odot$ (Dorman et al. 1993). On the other hand, models based on binary evolution predict a broader range of masses, from 0.3 to $0.8\,{\rm M}_\odot$ (Han et al. 2003). Hence an important step in understanding the origin of sdB stars is the determination of their mass distribution. A recent review of sdB stars is presented by Heber (2009).

There are currently 10 members of the HW Vir class, whose main features are summarized in Table 1. Among them, NSVS 14256825 (2MASS J2020+0437; hereafter referred to as NSVS 1425) is one of the least studied. It was discovered in the public data from the Northern Sky Variability Survey (Wozniak et al. 2004). The sole information on this system comes from the photometric data by Wils, di Scala & Otero (2007). These authors obtained *B, V* and I_C photometric light curves. The main parameters obtained by Wils et al. (2007) are listed in Table 1.

In this paper, we report on multiband photometry and phase-resolved optical spectroscopy of NSVS 1425. We present an improved solution for its geometrical and physical parameters and discuss these results in the context of HW Vir systems and their evolution.

2 OBSERVATIONS AND DATA REDUCTION

2.1 Optical and near-infrared photometry

The observations were carried out using the Observatório do Pico dos Dias/Laboratório Nacional de Astrofísica (OPD/LNA) facilities in Brazil. Photometric data in the *U, B, V,* R_C, I_C, *J* and *H* bands were obtained from 2010 July to November. Optical observations were performed using a CCD camera attached to the 0.6-m IAG telescope. Near-infrared (NIR) photometry data were collected by

★Based on observations carried out at the Observatório do Pico dos Dias/Laboratório Nacional de Astrofísica (OPD/LNA) in Brazil.

†E-mail: leonardo@das.inpe.br

Table 1. The currently known sdB+dM eclipsing binaries.

Name	T_1 (K)	M_1 ($M_{\odot}$)	M_2 ($R_{\odot}$)	R_1 ($R_{\odot}$)	R_2 ($R_{\odot}$)	$\log g_1$	Period (d)	Refs.	Notes
AA Dor	42 000	0.33/0.47	0.064/0.079	0.179/0.20	0.097/0.108	5.46	0.261	1,2,3	15,16
		0.25	0.054	0.165	0.089			4	16
NSVS 14256825	40 000	0.419	0.109	0.190	0.151	5.50	0.110 37	This work	15,16
	–	0.46	0.21	–	–	–	0.110 40	5	15
PG 1336−018	31 300	0.389	0.110	0.150	0.160	5.60	0.101 02	6	15,16
	32 740	0.459	–	–	–	–	–	7	17
2M 1533+3759	30 400	0.377	0.113	0.166	0.152	5.58	0.161 77	8	15,16
2M 1938+4603	29 564	0.48	0.12	–	–	5.425	0.125 76	9	15,16
HS 0705+6700	28 800	0.48	0.13	0.230	0.186	5.40	0.095 65	10	15,16
PG 1241−084	28 488	0.48	0.14	0.176	0.180	5.63	0.116 76	11	15
HS 2231+2441	28 370	0.47/0.499	0.075/0.072	0.250	0.127	5.39	0.110 59	12	15,16
SDSS J0820+0008	26 700	0.25/0.47	0.068/0.045	–	–	5.48	0.096	13	15,16
BUL SC16 335	–	–	–	–	–	–	0.125 05	14	15

(1) Heber (2009); (2) Klepp & Rauch (2011); (3) Hilditch et al. (2003); (4) Rucinski (2009); (5) Wils et al. (2007); (6) Vuĉković et al. (2009); (7) Charpinet et al. (2008); (8) For et al. (2010); (9) Østensen et al. (2010); (10) Drechsel et al. (2001); (11) Wood & Saffer (1999); (12) Østensen et al. (2007); (13) Geier et al. (2011); (14) Polubek et al. (2007); (15) Light Curves; (16) Spectroscopy; (17) Asteroseismology.

Table 2. Log of the photometric observations.

UT date	N	t_{exp} (s)	Telescope (m)	Filter
2010 July 30	300	20	0.6	R_C
2010 July 30	185	30	1.6	J
2010 July 31	250	30	0.6	B
2010 July 31	450	20	0.6	R_C
2010 July 31	177	30	1.6	J
2010 July 31	235	30	1.6	H
2010 August 1	235	40	0.6	U
2010 August 1	75	40	0.6	B
2010 August 1	100	30	1.6	Y
2010 August 1	215	30	1.6	J
2010 August 2	230	40	0.6	U
2010 August 2	400	20	0.6	I_C
2010 August 6	120	30	0.6	V
2010 August 7	220	30	0.6	V
2010 August 8	220	30	0.6	I_C
2010 August 9	160	25	0.6	R_C
2010 August 10	80	25	0.6	R_C
2010 August 18	800	10	0.6	R_C
2010 August 18	530	15	0.6	I_C
2010 August 19	225	40	0.6	U
2010 August 20	420	20	0.6	B
2010 September 1	160	30	0.6	V
2010 September 3	250	30	1.6	J
2010 September 4	142	50	1.6	J
2010 November 3	352	20	0.6	I_C

means of the CamIV imager attached to the 1.6-m Perkin–Elmer telescope.

The procedure to remove undesired effects from the CCD data included obtaining ∼100 bias frames and ∼30 dome flat-field images for each night of observations. The NIR flat-field images were produced using separate sequences of 30 ‘on’ and 30 ‘off’ exposures. The resulting of the ‘on’ image minus ‘off’ image was used as the master flat-field image. Table 2 summarizes the characteristics of the data collected for NSVS 1425. In this table, N is the number of individual images obtained with the integration time t_{exp}.

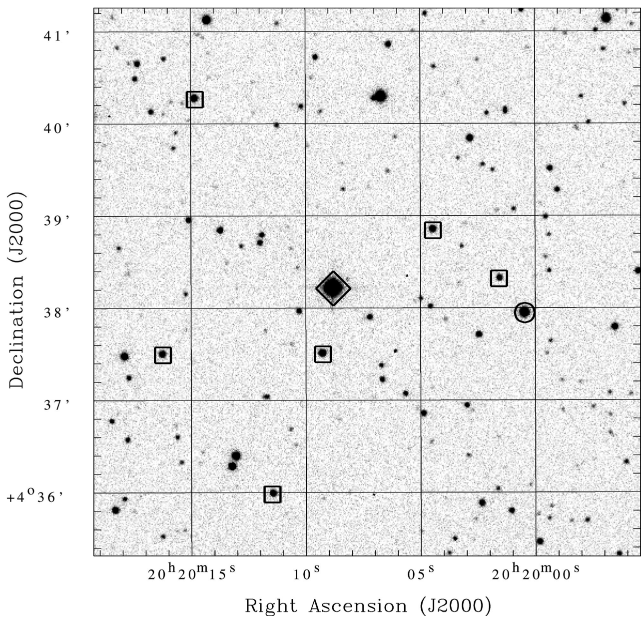

Figure 1. Finding chart for NSVS 14256825 in the R_C band obtained using the OPD/LNA 0.6-m telescope. The circle shows NSVS 1425, the diamond is the adopted reference star and the squares outline additional comparison stars.

The preparation of the CCD data was performed using standard IRAF[1] tasks (Tody 1993) and consisted of subtracting a master median bias image from each programme image, and then dividing the result by a normalized flat-field frame. In the J and H bands, additional steps of linearization and sky subtraction from dithered images were used in the preparation of the data. For both optical and infrared data, differential photometry was used to obtain the relative fluxes between the target and a set of constant flux stars in the field of view. As the NSVS 1425 field is not crowded, the extraction of the fluxes was carried out using aperture photometry. Fig. 1 shows a finding chart for NSVS 1425 with a reference star

[1] http://www.iraf.noao.edu

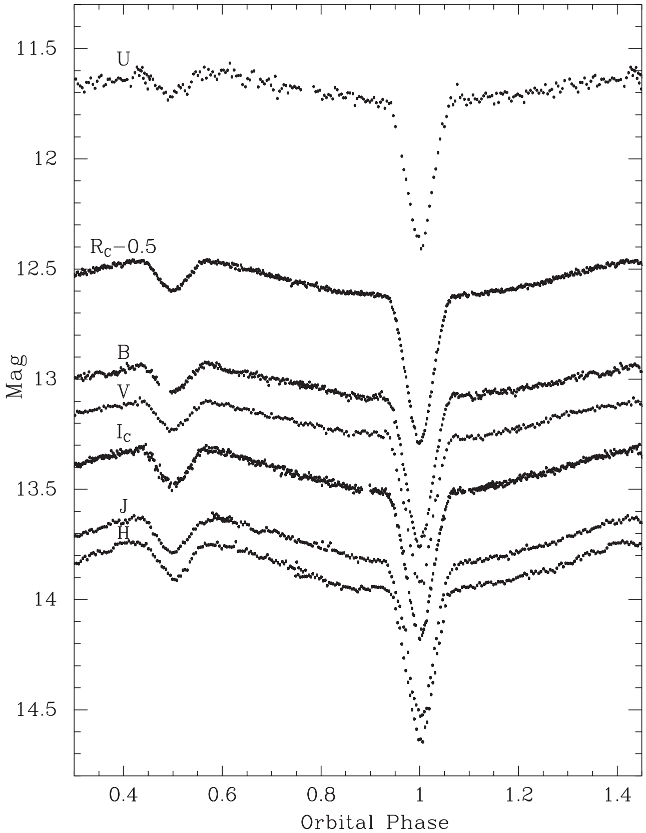

Figure 2. Calibrated NSVS 1425 light curves in the *U, B, V,* R_C, I_C, *J* and *H* bands folded on the 0.1104-d orbital period. The R_C-band curve was displaced upwards by 0.5 mag to improve visualization.

and a number of additional comparison stars adopted for differential photometry. Photometric standard stars were observed each night in order to calibrate the optical data. The NIR calibration is directly provided by the Two Micron All Sky Survey (2MASS) catalogue magnitudes for the reference and comparison stars. Fig. 2 shows a sample of calibrated light curves folded on the NSVS 1425 orbital period.

As can be seen from Fig. 2, the light curves of NSVS 1425 show a prominent reflection effect, which increases towards longer wavelengths. The depth of the primary eclipse is ∼0.7 mag and does not change significantly with wavelength, while the depth of the secondary eclipse increases towards longer wavelengths, from ∼0.1 mag in the *U* band to ∼0.18 mag in the *H* band. Table 3 shows the apparent magnitudes for NSVS 1425 at primary and secondary minima.

Table 3. Apparent magnitudes of NSVS 1425 at primary and secondary minima.

UT date	Band	Primary minimum	Secondary minimum
2010 August 2	*U*	12.41 ± 0.20	11.73 ± 0.20
2010 August 20	*B*	13.76 ± 0.15	13.06 ± 0.15
2010 August 7	*V*	13.93 ± 0.13	13.23 ± 0.13
2010 July 31	R_C	13.79 ± 0.12	13.10 ± 0.12
2010 August 18	I_C	14.18 ± 0.16	13.47 ± 0.16
2010 August 1	*J*	14.50 ± 0.24	13.80 ± 0.24
2010 July 31	*H*	14.60 ± 0.25	13.91 ± 0.25

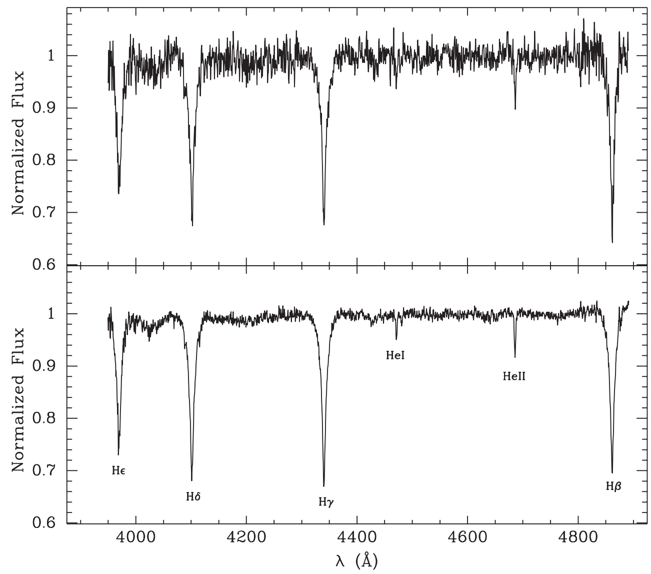

Figure 3. Upper panel: a normalized individual spectrum of NSVS 1425 with 900 s integration time. Lower panel: the average of 36 spectra after correcting for orbital motion.

2.2 Optical spectroscopy

The spectroscopic observations were performed using the Cassegrain spectrograph attached to the 1.6-m telescope at OPD/LNA. 36 spectra were obtained using the 1200 lines mm^{-1} grating and integration times of 10 or 15 min. The spectral coverage of this configuration is 3950–4900 Å, using 1.8 Å resolution [from the full width at half-maximum (FWHM) of the wavelength calibration lines]. 100 bias frames and 30 flat-field frames were obtained each night to remove systematic signatures from the CCD detector. Observations of a He–Ar comparison lamp were made every two exposures on the target to provide wavelength calibration. The spectrophotometric standard stars HR 1544, HR 7596 and HR 9087 (Hamuy et al. 1992) were observed for flux calibration.

The reduction of the spectra was carried out following the steps of bias subtraction, flat-field structure removal, optimal extraction, wavelength calibration and flux calibration using the standard routines in IRAF. The upper panel in Fig. 3 shows a typical normalized individual spectrum. The lower panel shows the average of all spectra after Doppler shifting using the radial-velocity orbital solution (see Section 3.2).

3 ANALYSIS AND RESULTS

3.1 Ephemeris

To determine an ephemeris for the times of the primary minimum in NSVS 1425, we combined our timings and those from Wils et al. (2007), after converting them to barycentric dynamical time (TDB). Our eclipse timings were obtained by modelling the primary eclipse using the Wilson–Devinney (WD) code (Wilson & Devinney 1971) together with a Markov chain Monte Carlo (MCMC) procedure (Gilks, Richardson & Spiegelhalter 1996) to obtain the uncertainties. The geometrical and physical parameters of the system are calculated as described in Section 3.4. These parameters were used as fixed inputs for the WD code and only the times of individual primary eclipses are left as free parameters. The median values and the 1σ uncertainties obtained from the marginal distribution of the fitted instants of minimum were adopted as the best values for location and error of each timing. Using the expression $T_{\rm min} = T_0 + EP$, where $T_{\rm min}$ are the predicted times of primary minimum, T_0 is a fiducial epoch, E is the cycle count from T_0 and P is the binary orbital period, we obtained the following ephemeris:

$$T_{\rm min} = {\rm TDB}\ 245\,4274.2087(1) + 0.110\,374\,230(2)E. \quad (1)$$

3.2 Radial-velocity solution

The radial velocities were obtained using the task FXCOR in IRAF. Initially, a combination of all 36 spectra was used as a template for the cross-correlation with the individual spectra. Regions around Hβ, Hγ, Hδ, Hϵ and He II λ4686 were selected (see Fig. 3) to improve the signal-to-noise ratio of the correlation procedure. The resulting radial-velocity solution was used to Doppler shift all individual spectra to the orbital rest frame. A better quality template is then produced from these rest-frame spectra. The procedure was iterated a number of times until the radial-velocity solution converged. Table 4 lists individual radial velocities and Fig. 4 shows the radial-velocity curve folded on the orbital phase together with the best solution for a circular orbit. The modelling provides a semi-amplitude $K_1 = 73.4 \pm 2.0\,{\rm km\,s^{-1}}$ and a systemic velocity $\gamma = -12.1 \pm 1.5\,{\rm km\,s^{-1}}$.

Table 4. Spectroscopic observations and radial velocities.

UT date	BJD (TDB) (245 0000+)	$t_{\rm exp}$ (s)	V (km s^{-1})	Orbital phase
2010 September 1	5441.482 56	900	2.29 ± 12.29	0.60
2010 September 1	5441.492 51	600	−8.05 ± 11.86	0.69
2010 September 1	5441.503 71	900	66.46 ± 10.50	0.79
2010 September 1	5441.517 99	900	12.46 ± 10.60	0.92
2010 September 1	5441.529 04	900	−40.38 ± 12.10	0.02
2010 September 1	5441.540 78	900	−67.43 ± 10.21	0.13
2010 September 1	5441.558 25	900	−83.52 ± 11.16	0.29
2010 September 1	5441.569 70	900	−64.55 ± 10.12	0.39
2010 September 1	5441.580 84	900	−21.99 ± 12.32	0.49
2010 September 1	5441.597 92	900	53.03 ± 12.84	0.65
2010 September 1	5441.609 20	900	60.29 ± 10.98	0.75
2010 September 1	5441.620 57	900	47.18 ± 9.33	0.85
2010 September 1	5441.638 57	900	−44.83 ± 10.33	0.02
2010 September 1	5441.652 59	900	−78.09 ± 12.25	0.14
2010 September 1	5441.663 64	900	−76.39 ± 12.18	0.24
2010 September 2	5442.424 78	900	−63.45 ± 10.09	0.14
2010 September 2	5442.435 81	900	−84.04 ± 10.91	0.24
2010 September 2	5442.453 06	900	−37.19 ± 9.84	0.40
2010 September 2	5442.464 13	900	−6.20 ± 8.10	0.50
2010 September 2	5442.481 16	900	44.56 ± 8.03	0.65
2010 September 2	5442.492 23	900	65.25 ± 9.62	0.75
2010 September 2	5442.513 04	900	32.99 ± 10.88	0.94
2010 September 2	5442.524 04	900	−32.57 ± 8.55	0.04
2010 September 2	5442.541 10	900	−82.53 ± 7.39	0.19
2010 September 2	5442.552 09	900	−77.39 ± 8.10	0.29
2010 September 2	5442.568 70	900	−30.80 ± 10.13	0.44
2010 September 2	5442.579 70	900	20.41 ± 10.04	0.54
2010 September 2	5442.600 86	900	57.22 ± 11.46	0.74
2010 September 2	5442.611 86	900	58.08 ± 9.66	0.83
2010 September 2	5442.628 93	900	−8.53 ± 10.40	0.98
2010 September 2	5442.639 92	900	-65.09 ± 9.83	0.09
2010 September 2	5442.656 64	900	−91.21 ± 10.98	0.24
2010 September 2	5442.667 63	900	−70.64 ± 11.55	0.34
2010 September 2	5442.684 42	900	−3.21 ± 6.66	0.49
2010 September 2	5442.695 42	900	23.22 ± 10.57	0.59
2010 September 2	5442.712 46	900	47.40 ± 9.12	0.74

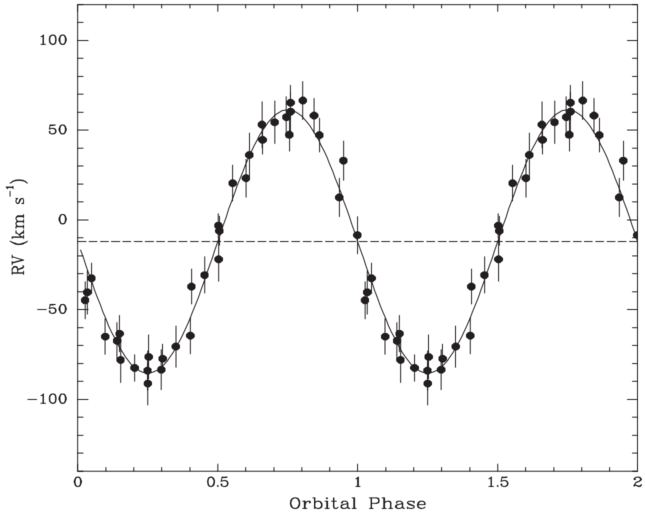

Figure 4. Radial velocity of the prominent lines in the spectra of NSVS 1425. The phases are calculated using the ephemeris presented in Section 3.1.

3.3 Atmospheric parameters

The atmospheric parameters of the sdB star can be determined using the Balmer and helium lines in the blue range of the spectrum. The spectra obtained in a 0.1 phase interval centred in the secondary eclipse, i.e. 0.45–0.55, were used to minimize the contribution of the reflection effect. Using χ^2 as the figure of merit, the combined spectrum was matched to a grid of synthetic spectra retrieved from the web page of TheoSSA.[2] The synthetic spectra were calculated by the Tübingen non-local thermodynamic equilibrium (NLTE) Model-Atmosphere Package[3] (TMAP). Two different metallicities were used: Model A with zero metallicity and Model B with the metallicity adopted by Klepp & Rauch (2011). The grid is composed of 26 values of effective temperatures, $30\,000 \le T \le 43\,000$ K with 500 K steps; 16 surface gravities, $5.2 \le \log g \le 6.0$ with 0.05 dex steps; and 10 helium abundances, $0.001 \le n({\rm He})/n({\rm H}) \le 0.01$ with 0.001 dex steps. All synthetic spectra were convolved with the projected rotational velocity $v \sin i = 73.4\,{\rm km\,s^{-1}}$ and with an instrumental profile of FWHM 1.8 Å.

The synthetic Balmer (Hβ to Hϵ) and helium (He I λ4471 and He II λ4686) lines were used in the fitting procedure to determine the effective temperature, surface gravity and He abundance. The best fit yields $T = 38\,000 \pm 500$ K, $\log g = 5.2 \pm 0.05$ and $n({\rm He})/n({\rm H}) = 0.003 \pm 0.001$ for Model A, and $T = 40\,000 \pm 500$ K, $\log g = 5.50 \pm 0.05$ and $n({\rm He})/n({\rm H}) = 0.003 \pm 0.001$ for Model B. Fig. 5 shows the observed spectra together with the best synthetic spectra for both models. The χ^2 of Model B is ∼5 per cent better than that of Model A.

[2] http://dc.g-vo.org/theossa

[3] http://astro.uni-tuebingen.de/̃rauch/TMAP/TMAP.html

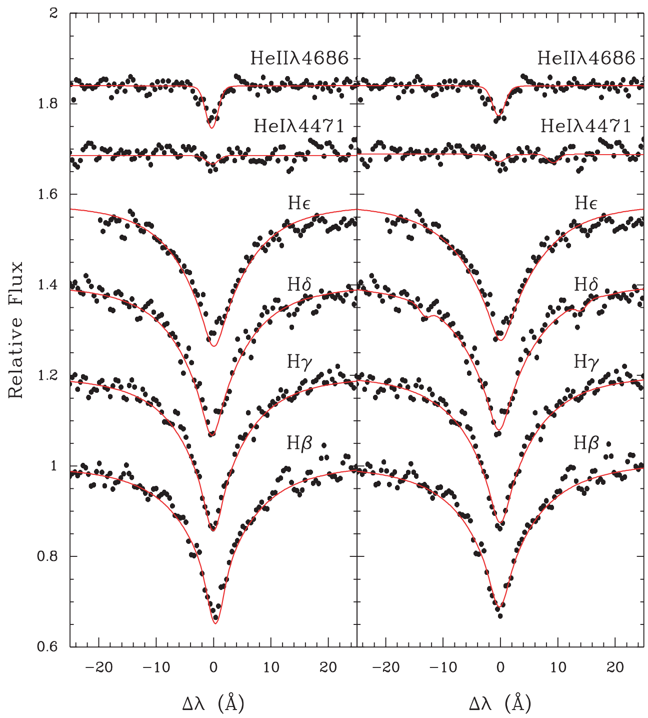

Figure 5. The best fits to the Balmer and helium lines used to derive effective temperature, surface gravity and helium abundance. The observed spectra are presented using black dots and the solid lines represent the best-fitting synthetic spectra. The left-hand and right-hand panels correspond to models with zero metallicity and the metallicity from Klepp & Rauch (2011), respectively.

3.4 Simultaneous modelling of light curves and radial velocities

In order to obtain the geometrical and physical parameters for NSVS 1425, we simultaneously analysed the *U, B, V*, R_C, I_C, *J* and *H* light curves and the radial-velocity curve using the WD code. The original WD code uses a differential correction method for improving an initial solution. This method works well if the initial parameter values are close to those corresponding to the optimal solution. However, if they are close to a local minimum, the differential correction procedure may fail to find the best solution. To solve this problem, the WD code was used as a 'function' to be optimized by the genetic algorithm PIKAIA(Charbonneau 1995), which is adequate to search for a global minimum in a model involving a large set of parameters.

To examine the marginal distribution of probability of the parameters and to establish realistic uncertainties, we used the solution obtained by PIKAIAas an input to an MCMC procedure.

Due to the large number of parameters to be fitted, it is important to constrain them using theoretical and spectroscopic information. From the spectroscopic analysis, we adopted the effective temperature of the primary star as an initial value. We can also constrain the mass ratio, q, using the mass function (equation 2) and assuming that the mass of the sdB star, M_1, is in the range of 0.1–0.8 $M_\odot$ (Driebe et al. 1998; Han et al. 2003), and that the radial-velocity semi-amplitude, K_1, is 73.4 km s^{-1}:

$$\frac{M_1(q \sin i)^3}{(1+q)^2} = 1.0361 \times 10^{-7}(1-e^2)^{3/2} K_1^3 P. \qquad (2)$$

As the components are in close orbit, the time-scales of synchronization and circularization are much shorter than the helium-burning lifetime (Zahn 1977). Thus, the orbit can be considered circular ($e = 0$) and the rotation of the components synchronized with the orbit. Finally, adopting the range of orbital inclinations for eclipsing binaries, $75^\circ < i < 90^\circ$, we obtained $0.21 < q < 0.45$ for the mass ratio range.

Mode 2 of the WD code, which sets no constraints on the Roche configuration, was used. The luminosity of the secondary star was computed assuming stellar atmosphere radiation. Linear limb-darkening coefficients, x_i, were used for both stars. Regarding the sdB star, we used the coefficients calculated by Díaz-Cordovés, Claret & Gimenez (1995) and Claret, Díaz-Cordovés & Gimenez (1995) for a star with effective temperature $T = 40\,000$ K and surface gravity $\log g = 5.0$. These are the closest values to those of the hot component in NSVS 1425 for which limb-darkening coefficients have been published in the literature. On the other hand, the linear limb-darkening coefficients of the cool star were left as free parameters, since the proximity of the hot star can significantly change these coefficients with respect to those of a single star. As the sdB star has a radiative envelope, its gravity-darkening exponent, β_1, and its bolometric albedo for reflective heating and reradiation, A_1, were set to unity (Rafert & Twigg 1980). The gravity-darkening exponent of the secondary component, β_2, was fixed at 0.3, which is appropriate for convective stars (Lucy 1967). As shown by For et al. (2010), Kilkenny et al. (1998) and Drechsel et al. (2001), the albedo of the secondary star, A_2, can assume physically unrealistic values $A_2 > 1$, especially at longer wavelengths where the reflected–reradiated light is more intense. For this reason, it was decided to perform two modellings: in Model 1, we adopt a constant (but free parameter) secondary albedo for all photometric bands; in Model 2, we consider variable and independent albedos for all photometric bands.

In both cases the remaining fitted parameters consist of: the mass ratio, $q = M_2/M_1$; the orbital inclination, i; the separation between the components, a; the Roche potentials, Ω_1 and Ω_2; and the effective temperatures of the two stars, T_1 and T_2.

In order to optimize the computational time, all light curves were binned with 160 s time resolution and the error of the bin average outside of the eclipses was assumed as the uncertainty. To test the goodness of fit, we use the reduced χ^2 defined as

$$\chi^2 = \frac{1}{n}\sum_i^n \left(\frac{O_i - C_i}{\sigma_i}\right)^2, \qquad (3)$$

where O_i are the observed points, C_i are the corresponding model, σ_i are the uncertainties at each point and n is the number of points. Fig. 6 shows the best fit together with the light and radial-velocity curves, while Table 5 lists the fitted and fixed parameters.

The values found for almost all parameters in the two models are consistent. However, the χ^2 for Model 2 is ~40 per cent better than for Model 1.

3.5 Fundamental parameters

Physical and geometrical parameters such as masses, radii and separation between the two components of the system can be derived from the solutions obtained in the previous sections. Substituting the values of the orbital period ($P_{orb} = 0.110\,374\,230$ d), semi-amplitude of the radial velocity ($K_1 = 73.4$ km s^{-1}), mass ratio ($q = 0.260$) and inclination ($i = 82\overset{\circ}{.}5$) in equation (2), $M_1 = 0.419 \pm 0.070\,M_\odot$ is obtained for the primary mass. The primary mass and

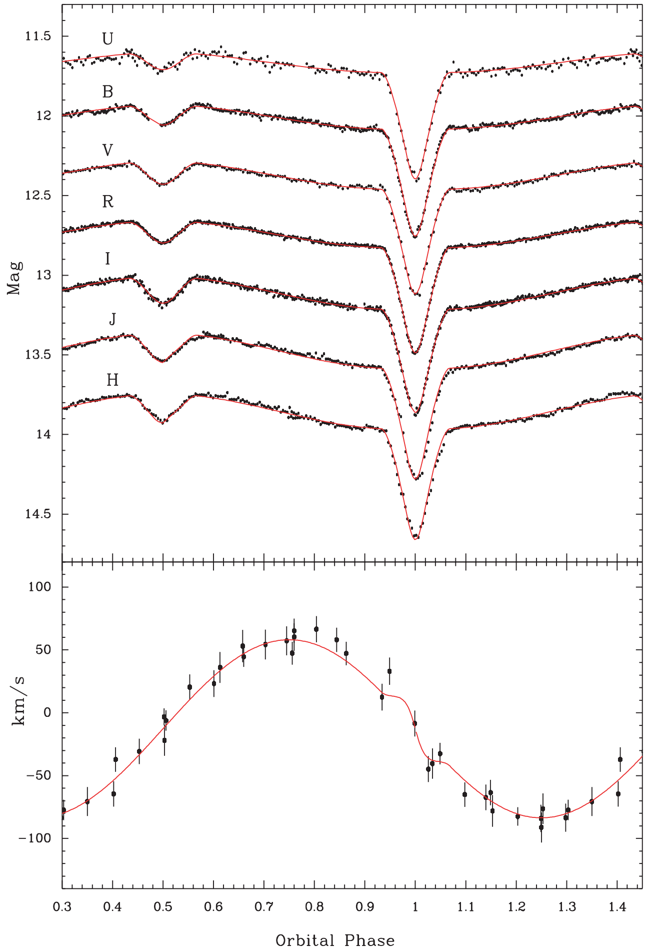

Figure 6. The best simultaneous fit for the U, B, V, R_C, I_C, J and H light curves and radial-velocity data using the WD code. The light curves are the same as those shown in Fig. 2 displaced vertically for better visualization.

the mass ratio are used to derive the secondary mass, $M_2 = 0.109 \pm 0.023\,M_{\odot}$. Using Kepler's third law, one can obtain the orbital separation, $a = 0.80 \pm 0.04\,R_{\odot}$, from which the absolute radii follow, $R_1 = 0.188 \pm 0.010\,R_{\odot}$ and $R_2 = 0.162 \pm 0.008\,R_{\odot}$. In Table 6 we show the fundamental parameters for NSVS 1425 derived from Model 1 and Model 2.

3.6 Rossiter–McLaughlin effect

An interesting spectroscopic signature in eclipsing binary systems is the Rossiter–McLaughlin (RM) effect (McLaughlin 1924; Rossiter 1924). This effect occurs when the eclipsed object rotates. There is evidence of this effect on the radial-velocity curve in the phase interval 0.95–1.05 (Fig. 6). Unfortunately, our data are not enough to model the RM effect to derive the alignment rotational parameters of the NSVS 1425 stars. However, our observed points are consistent with the predicted RM effect for aligned rotating stars obtained by the WD code with the parameters shown in Table 5.

Table 5. System parameters of the best fit for photometric light curves in U, B, V, R_C, I_C J and H bands and radial-velocity data for NSVS 1425.

Parameter	Model 1	Model 2
Fitted parameters		
$q = (M_2/M_1)$	0.28 ± 0.013	0.26 ± 0.012
i (°)	82.5 ± 0.4	82.5 ± 0.3
Ω_1^a	4.58 ± 0.13	4.55 ± 0.11
Ω_2^a	2.80 ± 0.15	2.69 ± 0.12
T_1 (K)	$42\,300 \pm 400$	$42\,000 \pm 500$
T_2 (K)	2400 ± 600	2550 ± 550
a^b ($R_{\odot}$)	0.74 ± 0.04	0.80 ± 0.04
$A_2^c(U)$	1.50 ± 0.11	2.0 ± 0.15
$A_2^c(B)$	1.50 ± 0.11	1.35 ± 0.13
$A_2^c(V)$	1.50 ± 0.11	1.20 ± 0.12
$A_2^c(R_C)$	1.50 ± 0.11	1.05 ± 0.09
$A_2^c(I_C)$	1.50 ± 0.11	1.3 ± 0.12
$A_2^c(J)$	1.50 ± 0.11	0.95 ± 0.14
$A_2^c(H)$	1.50 ± 0.11	1.10 ± 0.15
$x_2(U)$	0.64 ± 0.04	0.68 ± 0.04
$x_2(B)$	0.69 ± 0.04	0.74 ± 0.05
$x_2(V)$	0.78 ± 0.03	0.80 ± 0.04
$x_2(R_C)$	0.83 ± 0.02	0.87 ± 0.02
$x_2(I_C)$	0.90 ± 0.03	0.92 ± 0.03
$x_2(J)$	0.93 ± 0.04	0.95 ± 0.04
$x_2(H)$	0.98 ± 0.05	0.99 ± 0.05
Roche radii^g		
r_1 (pole)	0.231 ± 0.006	0.233 ± 0.005
r_1 (side)	0.233 ± 0.006	0.235 ± 0.005
r_1 (point)	0.235 ± 0.007	0.236 ± 0.006
r_1 (back)	0.234 ± 0.007	0.236 ± 0.006
r_2 (pole)	0.180 ± 0.016	0.194 ± 0.014
r_2 (side)	0.182 ± 0.016	0.198 ± 0.016
r_2 (point)	0.191 ± 0.019	0.210 ± 0.019
r_2 (back)	0.189 ± 0.019	0.207 ± 0.018
Fixed parameters		
A_1^c	1.0	1.0
β_1^d	1.0	1.0
β_2^d	0.3	0.3
$x_1^e(U)$	0.242	0.242
$x_1^e(B)$	0.233	0.233
$x_1^e(V)$	0.209	0.209
$x_1^f(R_C)$	0.176	0.176
$x_1^f(I_C)$	0.147	0.147
$x_1^f(J)$	0.112	0.112
$x_1^f(H)$	0.095	0.095
Goodness of fit		
χ^2	2.1	1.2

[a] Roche surface potential.
[b] Components separation.
[c] Bolometric albedo.
[d] Gravity-darkening exponent.
[e] Linear limb-darkening coefficient from Díaz-Cordovés et al. (1995).
[f] Linear limb-darkening coefficient from Claret et al. (1995).
[g] In units of orbital separation.

4 DISCUSSION

4.1 Characteristics of the primary star

Of all HW Vir systems, the primary of NSVS 1425 has the second highest temperature (see Table 1), consistent with the prominent He II λ4686 line (see Fig. 3). Accordingly, we suggest that the

Table 6. Fundamental parameters for NSVS 1425.

Parameter	Model 1	Model 2
M_1 ($M_\odot$)	0.346 ± 0.079	0.419 ± 0.070
M_2 ($M_\odot$)	0.097 ± 0.028	0.109 ± 0.023
R_1 ($R_\odot$)	0.173 ± 0.010	0.188 ± 0.010
R_2 ($R_\odot$)	0.137 ± 0.008	0.162 ± 0.008
T_1 (K)	$42\,300 \pm 500$	$42\,000 \pm 400$
T_2 (K)	2400 ± 500	2550 ± 500
$\log g_1$	5.50 ± 0.14	5.51 ± 0.11
$\log g_2$	5.15 ± 0.16	5.05 ± 0.13
a ($R_\odot$)	0.74 ± 0.04	0.80 ± 0.04

primary of NSVS 1425 is an sdBO star which means that this system is very similar to AA Dor and, hence, in a rare evolutionary stage (Heber 2009).

Comparing the values of $\log g$ derived from the simultaneous fit to photometric and spectroscopic data (Table 6) with those obtained from the modelling of the spectral lines of the primary star (Section 3.3), it is clear that the model with metallicity equal to that adopted by Klepp & Rauch (2011) provides consistent results, whereas the model with zero metallicity has a discrepancy. We noticed that the same kind of discrepancy had been found by Rauch (2000) in the analysis of the primary in AA Dor. Rauch (2000) obtained $\log g = 5.21$ from spectroscopic data, whereas Hilditch, Harries & Hill (1996) had derived $\log g = 5.53$ from photometric data modelling. This discrepancy was solved by Klepp & Rauch (2011) with the improvement of the Stark broadening modelling, the minimization of the reflection effect and adoption of metal-line blanketing.

4.2 Evolution

Han et al. (2003), from a detailed binary population synthesis study, presented three possible channels for forming sdB stars.

(i) *One or two phases of CE evolution*.
(ii) *One or two stable Roche lobe overflows*.
(iii) *A merger of two He-core white dwarfs*.

Driebe et al. (1998) and Heber et al. (2003) suggest another scenario to form an sdB star with low mass in binaries called post-red giant branch (RGB). This scenario is similar to the channel (i) proposed by Han et al. (2003), except that the resultant sdB in the first CE phase has insufficient mass in its core to ignite helium. However, it will evolve as a helium star through the sdB star region to form a helium-core white dwarf.

In Fig. 7 we compare the position of the primary component of NSVS 1425 on the ($T_{\rm eff}$, $\log g$) diagram with other sdB stars in short-period binary systems (see Table 1). We also show a sample of single sdB and sdOB stars analysed by Edelmann (2003). In the same graph we display evolutionary tracks for different masses in the post-EHB calculated by Dorman, Rood & O'Connell (1993) for single-star evolution. As can be seen, the position of the NSVS 1425 primary is close to that of the AA Dor primary. The evolutionary track for single-star evolution would only marginally explain the mass obtained for the sdB star in NSVS 1425. Out of the possible channels to form an sdB in binaries, we suggest that the channel (i) is probably the evolutionary scenario for NSVS 1425.

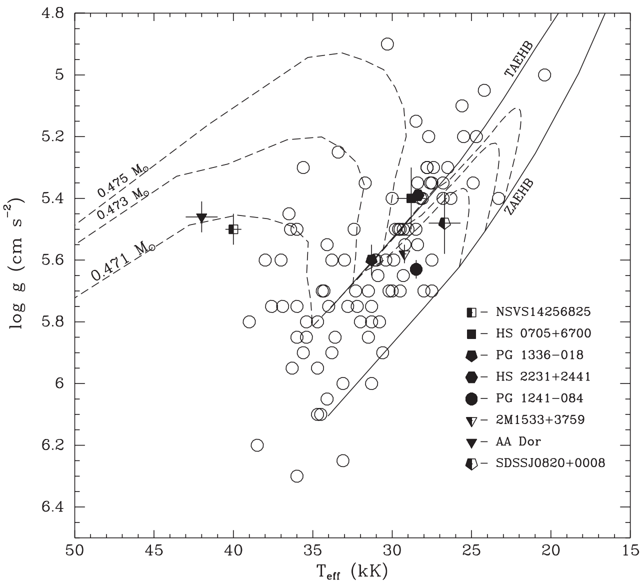

Figure 7. Position on the ($T_{\rm eff}$, $\log g$) diagram of the hot component of NSVS 1425 compared with other sdB stars (see Table 1). Isolated sdB and sdOB stars presented in Edelmann (2003) are shown with open circles. Dashed lines represent evolutionary tracks for different masses in the post-EHB evolution (Dorman et al. 1993). The zero-age extreme horizontal branch (ZAEHB) and terminal-age extreme horizontal branch (TAEHB) are represented by solid lines.

5 CONCLUSION

We present a photometric and spectroscopic analysis of the NSVS 1425 system. With a short orbital period, $P = 0.110\,374\,230(2)$ d, this binary shows both primary and secondary eclipses and a prominent reflection effect. From the spectroscopic analysis we obtain $73.4 \pm 2.0\,\mathrm{km\,s^{-1}}$ for the semi-amplitude of the radial velocity and $-12.1 \pm 1.5\,\mathrm{km\,s^{-1}}$ for the systemic velocity. The atmospheric parameters of the primary component (sdOB star), namely, effective temperature, $T = 40\,000 \pm 500$ K, surface gravity, $\log g = 5.5 \pm 0.05$ and helium abundance, $n(\mathrm{He})/n(\mathrm{H}) = 0.003 \pm 0.001$, were calculated matching the observed spectrum to a grid of NLTE synthetic spectra.

Simultaneously fitting the *U*-, *B*-, *V*-, $R_{\rm C}$-, $I_{\rm C}$-, *J*- and *H*-band light curves and radial-velocity curve using the WD code, the geometrical and physical parameters of NSVS 1425 were obtained. These results allow us to derive the absolute parameters of the system such as masses and radii of the components.

We compare the position of the sdB star in NSVS 1425 with other sdB and sdOB stars on the effective temperature versus surface gravity diagram. We describe the possible channels to form an sdB star in binaries and conclude that the post-CE development is probably the evolutionary scenario for NSVS 1425. The subsequent evolution of this system should lead to a cataclysmic variable. After a phase of angular momentum loss via gravitational radiation, this system will lie below the period gap of the cataclysmic variables.

ACKNOWLEDGMENTS

This study was partially supported by CAPES (LAA and JT), CNPq (CVR: 308005/2009-0) and Fapesp (CVR: 2010/01584-8). The TheoSSA service (http://dc.g-vo.org/theossa) used to retrieve theoretical spectra for this paper was constructed as part of the activities of the German Astrophysical Virtual Observatory. We acknowledge the use of the SIMBAD data base, operated at CDS, Strasbourg, France; the NASA's Astrophysics Data System Service; and the NASA's *SkyView* facility (http://skyview.gsfc.nasa.gov) located at NASA Goddard Space Flight Center.

REFERENCES

Charbonneau P., 1995, ApJS, 101, 309
Charpinet S., van Grootel V., Reese D., Fontaine G., Green E. M., Brassard P., Chayer P., 2008, A&A, 489, 377
Claret A., Díaz-Cordovés J., Gimenez A., 1995, A&AS, 114, 247
Díaz-Cordovés J., Claret A., Gimenez A., 1995, A&AS, 110, 329
Dorman B., Rood R. T., O'Connell R. W., 1993, ApJ, 419, 596
Drechsel H. et al., 2001, A&A, 379, 893
Driebe T., Schönberner D., Blöker T., Herwig F., 1998, A&A, 339, 123
Edelmann H., 2003, A&A, 400, 939
For B.-Q. et al., 2010, ApJ, 708, 253
Geier S. et al., 2011, ApJ, 731, L22
Gilks W. R., Richardson S., Spiegelhalter D. J. E., 1996, Markov Chain Monte Carlo in Practice. Chapman & Hall, London
Hamuy M., Walker A. R., Suntzeff N. B., Gigoux P., Heathcote S. R., Phillips M. M., 1992, PASP, 104, 533
Han Z., Podsiadlowski P., Maxted P. F. L., Marsh T. R., 2003, MNRAS, 341, 669
Heber U., 2009, ARA&A, 47, 211
Heber U., Edelmann H., Lisker T., Napiwotzki R., 2003, A&A, 411, L477
Hilditch R. W., Harries T. J., Hill G., 1996, MNRAS, 279, 1380
Hilditch R. W., Kilkenny D., Lynas-Gray A. E., Hill G., 2003, MNRAS, 344, 644
Kilkenny D., O'Donoghue D., Koen C., Lynas-Gray A. E., van Wyk F., 1998, MNRAS, 296, 329
Klepp S., Rauch T., 2011, A&A, 531, L7
Lucy L. B., 1967, Z. Astrophys., 65, 89
McLaughlin D. B., 1924, AJ, 60, 22
Østensen R., Oreiro R., Drechsel H., Heber U., Baran A., Pigulski A., 2007, in Napiwotzki R., Burleigh M. R., eds, ASP Conf. Ser. Vol. 372, 15th European Workshop on White Dwarfs. Astron. Soc. Pac., San Francisco, p. 483
Østensen R. H. et al., 2010, MNRAS, 408, L51
Polubek G., Pigulski A., Baran A., Udalski A., 2007, in Napiwotzki R., Burleigh M. R., eds, ASP Conf. Ser. Vol. 372, 15th European Workshop on White Dwarfs. Astron. Soc. Pac., San Francisco, p. 487
Rafert J. B., Twigg L. W., 1980, MNRAS, 193, 79
Rauch T., 2000, A&A, 356, 665
Rossiter R. A., 1924, ApJ, 60, 15
Rucinski S. M., 2009, MNRAS, 395, 2299
Taam R. E., Ricker P. L., 2010, New Astron. Rev., 54, 65
Tody D., 1993, in Hanisch R. J., Brissenden R. J. V., Barnes J., eds, ASP Conf. Ser. Vol. 52, Astronomical Data Analysis Software and Systems II. Astron. Soc. Pac., San Francisco, p. 173
Vuĉković M., Østensen R. H., Aerts C., Telting J. H., Heber U., Oreiro R., 2009, A&A, 505, 239
Wils P., di Scala G., Otero S. A., 2007, Inf. Bull. Var. Star, 5800, 1
Wilson R. E., Devinney E. J., 1971, ApJ, 166, 605
Wood J. H., Saffer R., 1999, MNRAS, 305, 820
Woźniak P. R., Williams S. J., Vestrand W. T., Gupta V., 2004, AJ, 128, 2965
Zahn J.-P., 1977, A&A, 57, 383

This paper has been typeset from a TEX/LATEX file prepared by the author.